Dalton Transactions

Cite this: *Dalton Trans.*, 2011, **40**, 12742

www.rsc.org/dalton

PAPER

Isomorphous Co(II) and Ni(II) antiferromagnets based on mixed azide- and carboxylate-bridged chains: metamagnetism and single-chain dynamics†

Xiu-Mei Zhang,[a,b] Kun Wang,[a] Yan-Qin Wang[a] and En-Qing Gao*[a]

Received 7th June 2011, Accepted 2nd September 2011
DOI: 10.1039/c1dt11068c

Two isomorphous Co(II) and Ni(II) coordination polymers with azide and the 4-(4-pyridyl)benzoic acid *N*-oxide ligand (4,4-Hopybz) were synthesized, and structurally and magnetically characterized. They are formulated as $[M(4,4\text{-opybz})(N_3)(H_2O)]_n$ (M = Co, **1** and Ni, **2**). The compounds consist of 2D coordination networks, in which 1D coordination chains with (μ-N_3)(μ-COO) bridges are interlinked by the 4,4-opybz spacers, and the structure also features intra- and interchain O–H···O hydrogen-bonding bridges between metal ions. Both compounds exhibit ferromagnetic interactions through the intrachain (μ-N_3)(μ-COO)(O–H···O) bridges and antiferromagnetic interactions through the interchain O–H···O bridges. The ferromagnetic chains are antiferromagnetically ordered, and the antiferromagnetic phases exhibit field-induced metamagnetic transition. It is found that **1** displays slow relaxation of magnetization, typical of single-chain magnets, while **2** does not. The difference emphasizes the great importance of large magnetic anisotropy for single-chain-magnet dynamics.

Introduction

Molecular magnetic materials have been one of the most active topics for decades.[1,2] The huge diversity and versatility of coordination and supramolecular chemistry have provided great opportunities to obtain new magnetic materials and to better understand fundamental magnetic phenomena. Field-induced metamagnets are a special type of antiferromagnets in which the weak antiferromagnetic (AF) order between magnetic chains or layers can be broken up by an applied field to induce a first-order transition,[3] while single-chain magnets (SCMs) are magnetizable 1D systems exhibiting slow dynamics of magnetization.[4–6] They both require strong magnetic correlations to generate ferromagnetic (FM), ferrimagnetic or spin-canted AF chains (and layers for metamagnets). Large uniaxial magnetic anisotropy is required for SCMs, and interchain interactions may impede SCM dynamics. By contrast, weak interchain/interlayer AF interactions are required for metamagnets.[3a] Generally speaking, the requirements of SCMs are more difficult to meet, and sometimes the attempts to obtain SCMs led to metamagnets.[7] Interestingly, it has been recently demonstrated that metamagnetism and SCM dynamics can coexist, but the examples are still very limited.[8,9]

Recently we have been investigating magnetic systems with simultaneous carboxylate and azide bridges. We have established an efficient synthetic approach to such systems: making use of zwitterionic mono- or dicarboxylate ligands to facilitate the simultaneous coordination of carboxylate and azide.[7a,9–11] Bifunctional ligands bearing carboxylate and pyridyl or pyridyl-*N*-oxide coordinative groups have also been used to construct simultaneous bridging systems, but the study using the pyridyl-*N*-oxide derivatives has only been limited to the simple pyridylcarboxylate-*N*-oxide.[7d,12] Noticeably, the simultaneous bridges usually induce FM interactions in Co(II) and Ni(II) systems, some of which are composed of FM chains and display metamagnetic and/or SCM properties.[7,9,13] To extend the study, here we report the structures and magnetic properties of two isomorphous compounds of formula $[M(4,4\text{-opybz})(N_3)(H_2O)]_n$ (4,4-opybz = 4-(4-pyridyl)benzoate *N*-oxide, M = Co, **1** and Ni, **2**). They consist of 2D coordination layers in which 1D chains with [(N_3)(COO)] double bridges are interlinked by 4,4-opybz ligands, and the structure is reinforced by intra- and interchain O–H···O hydrogen bond bridges between the metal ions. Magnetically, both compounds exhibit intrachain FM interactions, AF order, and field-induced metamagnetism. However, the different metal ions lead to dramatic differences in dynamic properties: **1** shows complex relaxation dynamics related to the SCM components, while **2** does not.

Experimental

Materials and physical measurements

The reagents were obtained from commercial sources and used without purification. The ligand (4,4-Hopybz) was prepared according to a procedure for similar compounds.[14]

[a]*Shanghai Key Laboratory of Green Chemistry and Chemical Processes, Department of Chemistry, East China Normal University, Shanghai, 200062, China. E-mail: eqgao@chem.ecnu.edu.cn*
[b]*School of Chemistry and Materials Science, Huaibei Normal University, Huaibei, Anhui, 235000, China*

† Electronic supplementary information (ESI) available: Supplementary graphics. CCDC reference number 826223 (**1**). For ESI and crystallographic data in CIF or other electronic format see DOI: 10.1039/c1dt11068c

Elemental analyses were determined on an Elementar Vario ELIII analyzer. The FT-IR spectra were recorded in the range 500–4000 cm^{-1} using KBr pellets on a Nicolet NEXUS 670 spectrophotometer. Temperature- and field-dependent magnetic measurements were performed on a Quantum Design MPMSXL5 SQUID magnetometer. The experimental susceptibilities were corrected for the diamagnetism of the constituent atoms (Pascal's tables).[15]

Synthesis

$[Co(4,4\text{-opybz})(N_3)(H_2O)]_n$ (1). A mixture of $CoCl_2{\cdot}6H_2O$ (0.1 mmol, 0.024 g), NaN_3 (0.5 mmol, 0.032 g), and 4,4-Hopybz (0.025 mmol, 0.0062 g) was dissolved in H_2O (3 ml) in a Teflon-lined stainless steel vessel (25 ml), heated at 70 °C for 3 days under autogenous pressure, and then cooled to room temperature. Purple plate crystals of **1** were obtained in a yield of 83% based on 4,4-Hopybz. Anal. (%): Found: C, 43.41; H, 3.39; N, 16.55. Calc. for $C_{12}H_{10}CoN_4O_4$: C, 43.26; H, 3.03; N, 16.82. Main IR bands (KBr, cm^{-1}): 2062s [$\nu(N_3)$], 1593m [ν_{as}(COO)], 1560m, 1521m, 1477w, 1398s [ν_s(COO)], 1186m, 851m, 777w.

$[Ni(4,4\text{-opybz})(N_3)(H_2O)]_n$ (2). A procedure similar to that for **1** was followed to prepare **2** using $NiCl_2{\cdot}6H_2O$ instead of $CoCl_2{\cdot}6H_2O$. Green polycrystals of **2** were obtained in a yield of 78% based on 4,4-Hopybz. Our attempts to get single crystals of **2** by different methods were fruitless. Anal. (%): Found: C, 43.50; H, 3.49; N, 17.26. Calc. for $C_{12}H_{10}NiN_4O_4$: C, 43.29; H, 3.03; N, 16.83. Main IR bands (KBr, cm^{-1}): 2060s [$\nu(N_3)$], 1596m [ν_{as}(COO)], 1564m, 1516m, 1483w, 1386s [ν_s(COO)], 1199m, 850m, 646w.

Crystal structure analysis

Diffraction data for **1** was collected at 293 K on a Bruker Apex II CCD area detector equipped with graphite-monochromated Mo-Kα radiation (λ = 0.71073 Å). Empirical absorption corrections were applied using the SADABS program.[16] The structures were solved by direct methods and refined by the full-matrix least-squares method on F^2, with all non-hydrogen atoms refined with anisotropic thermal parameters.[17] All the hydrogen atoms attached to carbon atoms were placed in calculated positions and refined using the riding model, and the water hydrogen atoms were located from the difference maps. Selected crystal data are listed in Table 1.

Table 1 Crystal data and structure refinement for compound **1**

Compound	**1**
Formula	$C_{12}H_{10}CoN_4O_4$
M_r	333.17
Crystal system	Monoclinic
Space group	$P2_1/c$
a/Å	7.2227(7)
b/Å	26.181(2)
c/Å	14.2067(12)
β/°	106.151(4)
V/Å^3	2580.4(4)
Z	8
D_c/g cm^{-3}	1.715
μ/mm^{-1}	1.353
Unique reflections	5025
R_{int}	0.0365
$R1$ [$I > 2\sigma(I)$]	0.0348
$wR2$ (all data)	0.0856

Powder X-ray diffraction

Powder X-ray diffraction data for **1** and **2** were collected on a Bruker D8-ADVANCE diffractometer equipped with Cu-Kα radiation (λ = 1.5406 Å) at a scan speed of 2° min^{-1} in the 2θ range of 5–35°. Since the patterns of **1** and **2** are very similar, the unit cell parameters of **2** were refined in the $P2_1/c$ space group using the CELREF program,[18] with the parameters of **1** as initial values. A total of 40 reflections were used in the refinements, and the final refinement gave a = 7.299(9), b = 25.87(2), c = 14.02(2) Å, β = 105.7(1)° and V = 2548(5) Å^3 with $R = (\sum(2\theta_{obs} - 2\theta_{cald})^2/N_{ref})^{1/2}$ = 0.0309.

Results and discussion

Crystal structures

Single-crystal X-ray analyses revealed that compound **1** consists of 2D layers in which 1D $[Co(N_3)(COO)]_n$ chains are connected by the 4,4-opybz spacers. Selected bond lengths and angles are summarized in Table 2. There are three crystallographically independent Co^{II} ions. The Co1 ion assumes the octahedral $[N_2O_4]$ geometry defined by two *transoid* carboxylate oxygen atoms (O1, O4), two *cisoid* coordinated water molecules (O7, O8) and two *cisoid* azide nitrogen atoms (N3, N6). The Co1–N (O) distances range from 2.064(2) to 2.162(2) Å. The Co2 and Co3 are located at different inversion centers in similar *trans*-octahedral $[N_2O_4]$ environments, with only minor differences in bond parameters. Four oxygen atoms (two from carboxylate groups and two from *N*-oxide groups) define an equatorial plane, with the axial sites occupied by two azide nitrogen atoms. The equatorial Co–O distances are somewhat shorter than the Co–N ones. The metal ions alternate in the –Co1–Co2–Co1–Co3– repeating sequence, and the adjacent metal ions are doubly bridged by a carboxylate group in the *syn*,*syn* mode and an azide ligand in the end-on (EO) mode, generating a 1D chain along the [101] direction (Fig. 1). The two double bridges between Co1 and Co2 and between Co1 and Co3 are somewhat different in terms of their structural parameters. The [Co1(COO)(N_3)Co2] moiety has a Co–N–Co bridging angle of 123.3(1)°, a Co–O···O–Co torsion angle of 27.6(1)°, and a Co···Co distance of 3.778(4) Å, while the corresponding parameters for the [Co1(COO)(N_3)Co3] moiety are 120.4(1)°, 35.8(1)° and 3.704(5) Å, respectively. It is noted

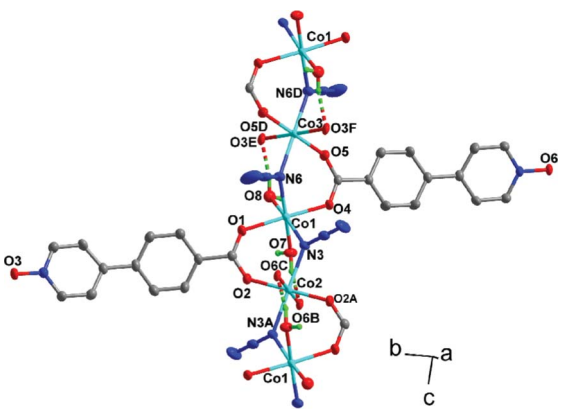

Fig. 1 A chain structure with azide, carboxylate and hydrogen bonding bridges in **1**.

Table 2 Selected bond lengths (Å) and angles (°) for compound **1**

Co1–O4	2.064(2)	Co1–O1	2.097(2)	Co2–O2	2.070(2)	Co2–O6B	2.115(2)
Co1–O7	2.103(2)	Co1–N6	2.119(2)	Co2–N3	2.132(2)	Co3–O5	2.079(2)
Co1–O8	2.154(2)	Co1–N3	2.162(2)	Co3–O3E	2.128(2)	Co3–N6	2.148(2)
O4–Co1–O1	177.62(8)	O4–Co1–O7	86.70(1)	O6B–Co2–O6C	180.00(9)	O2–Co2–N3	90.11(8)
O1–Co1–O7	90.92(8)	O4–Co1–N6	91.95(8)	O2–Co2–N3A	89.89(8)	O6C–Co2–N3	88.57(8)
O1–Co1–N6	90.41(8)	O7–Co1–N6	171.46(8)	O6B–Co2–N3	91.43(8)	N3A–Co2–N3	180.000(1)
O4–Co1–O8	89.91(7)	O1–Co1–O8	89.62(7)	O5–Co3–O5D	180.00(5)	O5–Co3–O3F	87.26(7)
O7–Co1–O8	78.94(7)	N6–Co1–O8	92.63(8)	O5–Co3–O3E	92.74(7)	O3E–Co3–O3F	180.00(8)
O4–Co1–N3	88.28(8)	O1–Co1–N3	91.68(8)	O5–Co3–N6	90.81(8)	O5–Co3–N6D	89.19(8)
O7–Co1–N3	88.79(8)	N6–Co1–N3	99.61(9)	O3F–Co3–N6	88.84(8)	O3E–Co3–N6	91.16(8)
O8–Co1–N3	167.68(8)	O2A–Co2–O2	180.000(1)	N6–Co3–N6D	180.0	Co2–N3–Co1	123.3(1)
O2–Co2–O6C	95.25(7)	O2–Co2–O6B	84.75(7)	Co1–N6–Co3	120.4(1)		

Symmetry codes: (A) $-x+1, -y, -z+2$; (B) $x, -y+1/2, z+1/2$; (C) $-x+1, y-1/2, -z+3/2$; (D) $-x+1, -y, -z+1$; (E) $-x+1, y+1/2, -z+3/2$; (F) $x, -y-1/2, z-1/2$.

that the chain structure is reinforced by two sets of intrachain hydrogen bonds between the coordinated water molecules (O7 and O8) and the coordinated *N*-oxide oxygen atoms (O6B and O3E) (Fig. 1), with O7–H7C···O6B = 168.5(1)°, H···O = 1.772(3) Å, O7···O6 = 2.678(4) Å; and O8–H8C···O3E = 169.9(1)°, H···O = 1.778(3) Å, O8···O3 = 2.625(5) Å. The hydrogen bonds provide triatomic O–H···O bridges between adjacent Co(II) ions, and therefore, it can be stated that the Co(II) ions are linked by the triple [(μ-COO)(μ-EO-N_3)(O–H···O)] bridges.

The coordinated water molecules (O7 and O8) also form interchain hydrogen bonds. The O8 water molecule as donor is hydrogen-bonded to an azide nitrogen atom (N5) from another chain with O8–H8B···N5 ($1+x, y, z$) = 165.3(2)°, H···N = 2.165(3) Å and O8···N5 = 2.992(4) Å, while the O7 water molecule forms a hydrogen bond with an *N*-oxide oxygen atom (O6) from another chain, with O7–H7B···O6 ($2-x, -0.5+y, 1.5-z$) = 161.3(2)°, H···O = 2.033(3) Å and O7···O6 = 2.850(4) Å. Noticeably, the latter hydrogen bond builds up a short triatomic O–H···O bridge between Co(II) ions from different chains, with a relatively short Co···Co distance of 5.98(1) Å. This feature may be relevant to magnetic behaviors. The interchain hydrogen bonds serve to interlink the $[Co(COO)(N_3)]_n$ chain into a 2D sheet along the *ac* plane (Fig. 2a). The sheet features an eight-membered hydrogen-bonded ring with graph set $R_4^2(8)$,[19] which is formed from two pairs of triatomic O–H···O bridges involving two water molecules and two *N*-oxide oxygen atoms from different coordination chains.

The 4,4-opybz ligand serves as a μ_3 bridge, with the *syn*,*syn* carboxylate group binding two metal ions from one chain and the *N*-oxide group binding a metal ion from another chain, Thus the chains are interlinked into a 2D layer along the $(10\bar{1})$ plane (Fig. 2b). The nearest interchain Co···Co distance spanned by the 4,4-opybz ligand is 13.090(1) Å. The coordination layers are stacked into a 3D structure through the above-mentioned O–H···N and O–H···O hydrogen bonds (Fig. S1, ESI†). Alternatively, the 3D structure may be described as a layer-pillared structure with hydrogen-bonded layers (Fig. 2a) and organic pillars (the backbones of the 4,4-opybz ligands) (Fig. S2, ESI†).

We failed in obtaining single crystals of **2** for X-ray crystallographic analysis. However, the PXRD pattern of **2** is in good agreement with that calculated from the single-crystal data of **1**

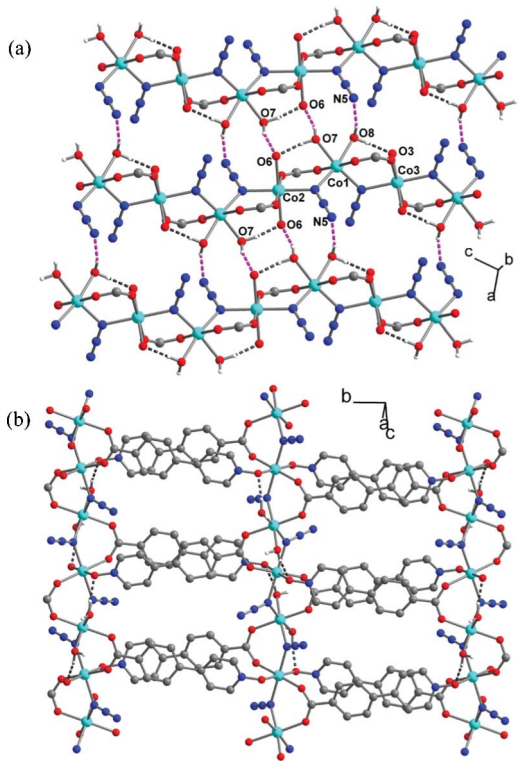

Fig. 2 (a) 2D sheet through hydrogen bonds. The dashed lines represent the intrachain (grey) and interchain (purple) hydrogen bonds. (b) 2D network formed by the 4,4-opybz ligands connecting the chains with mixed bridges.

(Fig. 3), indicating that **2** is isomorphic with **1**. The peaks observed for **2** can be indexed in the same space group with similar cell parameters. The cell volume of **2** is slightly smaller than that of **1**, as expected from the smaller radius of Ni(II) compared to Co(II).

Magnetic properties

Compound 1. The magnetic susceptibility (χ) of compound **1** was measured using powdered crystals under 1 kOe in the range of 2–300 K (Fig. 4). The χT value per Co(II) at 300 K is about 3.64 emu K mol^{-1}, falling within the usual range for octahedral Co(II) with an unquenched orbital momentum. As the temperature is

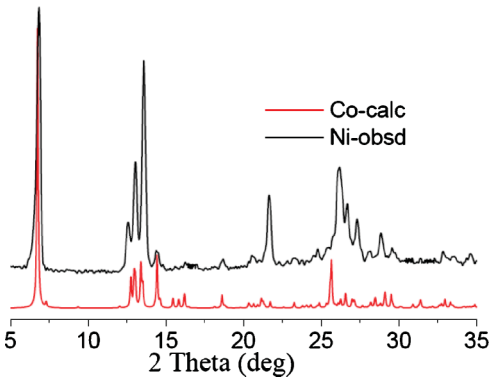

Fig. 3 Comparison of the XRD pattern measured for **2** (black) with that calculated from the single-crystal data of **1** (red).

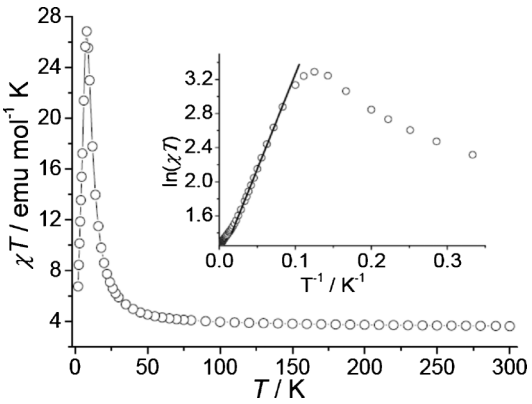

Fig. 4 Temperature dependence of χT for **1**. Inset: $\ln(\chi T)$ *vs.* $1/T$ plots, the solid line representing the linear fit.

lowered, the χT value increases continuously to a maximum at 8.0 K and then drops rapidly. The data above 30 K follow the Curie–Weiss law with C = 3.50 emu K mol^{-1} and θ = 11.8 K. The behaviors evidently indicate the presence of intrachain FM interactions.

It is well known that the correlation length (ξ) of a 1D FM chain with uniaxial anisotropy diverges exponentially with temperature: $\xi \propto \chi T \approx C\exp(\Delta_\xi/T)$ (where Δ_ξ is the exchange energy cost to create a domain wall along the chain), which suggests a linear variation of $\ln(\chi T)$ with $1/T$.[1c,20] The $\ln(\chi T)$ *vs.* $1/T$ plot for **1** (Fig. 4 inset) displays a linear region between 12 and 35 K with a slope of Δ_ξ = 22.3 K, confirming the uniaxially anisotropic character of the chain. According to the Ising-chain model with uniform magnetic exchange ($\mathbf{H} = -JS^2\sum\boldsymbol{\sigma}_i\boldsymbol{\sigma}_{i+1}$, where $\sigma_i = \pm 1$), Δ_ξ is related to magnetic exchange by $\Delta_\xi = 2JS^2$.[1c,21] In our case, handling Co(II) at low temperature as an $S = 1/2$ effective spin, we obtained J = 44.6 K (31.0 cm^{-1}). Since the structural data reveal alternating bridging motifs along the chain, we have attempted to evaluate the alternating magnetic interactions using a two-J Ising-chain model,[22] but the best fits in appropriate temperature ranges (from 35 to 12 K or lower) led to two widely different parameters (*e.g.*, 20 and 64 cm^{-1}), which seem to be unrealistic because the two bridging motifs have similar structural parameters.

The $\ln(\chi T)$ *vs.* $1/T$ plot deviates significantly from linearity at lower temperature and shows a maximum at 8.0 K. This may be due to saturation effects and interchain AF interactions. As will be shown by low-field dc and zero-field ac measurements (see below), the FM chains are long-range ordered by interchain AF interactions.

The isothermal magnetization behaviors from 0 to 5 T were measured at 2 K (Fig. 5a). The overall rise of magnetization upon increasing the field to 4 kOe is much more rapid than expected for isolated Co(II) systems, confirming the presence of FM coupling between Co(II) ions. The magnetization increases slowly and quasi-linearly in the high-field range and shows no indication of saturation even at the high field of 5 T, attributable to the large magnetic anisotropy of the octahedral Co(II) system. Moreover, the low-field region of the magnetization curve shows a sigmoid shape, indicative of field-induced metamagnetism: the FM chains are long-range ordered in an AF phase at zero field, and the AF order can be broken up by an applied field. The critical field, corresponding to the maximum position in the $(\mathrm{d}M/\mathrm{d}H)$–$H$ plot, is estimated to be 950 Oe at 2 K (Fig. 5a inset). The magnetization loop measured by cycling the field between 5 and −5 T at 2 K shows the double sigmoid shape typical of metamagnets. Narrow hysteresis was observed in the AF region, with very small coercive field and remnant magnetization at zero field (Fig. 5b).

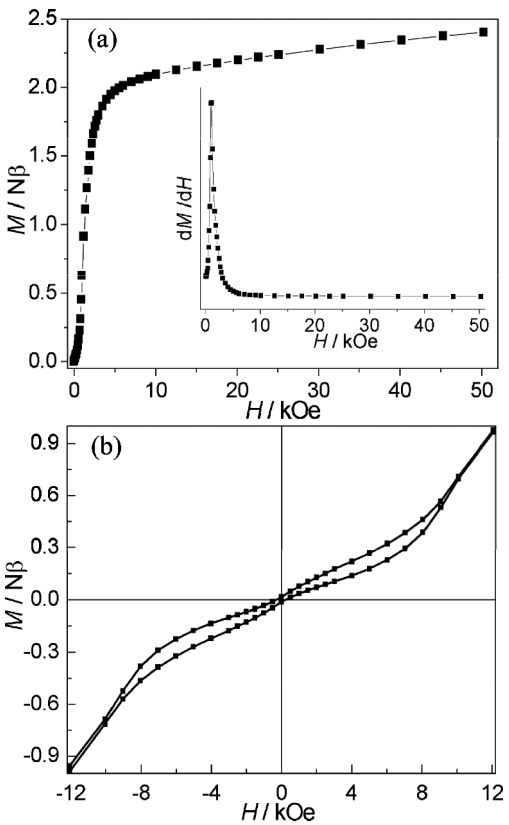

Fig. 5 (a) Plots of M *vs.* H and $\mathrm{d}M/\mathrm{d}H$ *vs.* H (inset) for **1** at 2 K. (b) Magnetic hysteresis at 2 K.

To confirm the metamagnetic behaviours, field-cooled (FC) magnetization measurements were performed under different fields. The FC curves under low field (20 Oe in Fig. 6a) show a maximum at about 7.9 K, supporting the occurrence of AF ordering. When the external field is increased (Fig. 6b), the maximum value shifts toward low temperature and finally disappears, confirming the field-induced phase transition from AF to FM.

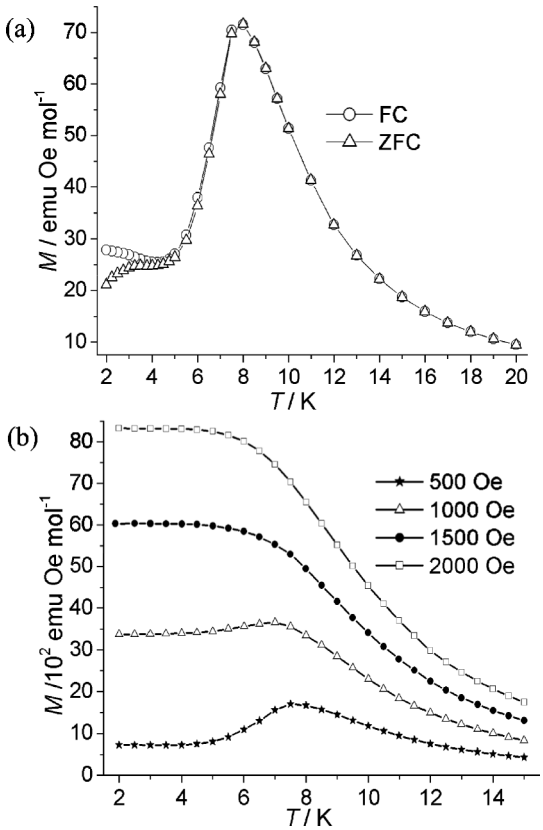

Fig. 6 (a) ZFC and FC magnetization curves of **1** at 20 Oe. (b) FC magnetization curves of **1** at different fields.

The zero-field-cooled (ZFC) magnetization at 20 Oe is also measured. As shown in Fig. 6a, the ZFC and FC magnetization curves diverge below about 5 K. The magnetization irreversibility is unusual for an AF ordered phase. To gain insight into the origin of the magnet-like irreversibility, thermal ac susceptibility measurements (Fig. 7) were performed on **1** under a zero dc field with a driving ac field 3.5 Oe oscillating at different frequencies.

As shown in Fig. 7, the real component (χ') of the ac susceptibility exhibits a frequency-independent maximum at 7.7 K, while the imaginary component (χ'') is zero down to 6 K. The phenomenon is typical of antiferromagnets. However, at lower temperature, the χ' plots display shoulders and meanwhile the χ'' data become nonzero and show peaks. Both components are strongly dependent upon frequency, with the χ'' maximum shifting from 3.6 K at 997 Hz to <2 K at 1 Hz, suggesting the occurrence of slow magnetization relaxation in the AF phase. The frequency dependence is measured by $\phi = (\Delta T_p/T_p)/\Delta(\log f) \approx 0.15$ (T_p is the temperature at which χ'' reaches a maximum). This value is out of the range for spin glass ($\phi \leq 0.08$)[23] but consistent with superparamagnets including SCMs ($0.1 \leq \phi \leq 0.3$).[23,24] The relaxation time $\tau(T)$ data derived from the $\chi''(T)$ peaks can be fitted to the Arrhenius law $\tau = \tau_o \exp(\Delta_\tau/T)$ (Fig. 7 inset), with $\tau_o = 2.44 \times 10^{-8}$ s and $\Delta_\tau = 32.0$ K (Δ_τ is the energy barrier to reverse the magnetization), suggesting a thermally activated mechanism of the magnetic relaxation. The τ_o and Δ_τ values lie in the typical range for superparamagnets including SCMs.[4a,24] Notably, the $\chi''(T)$ peaks are dissymmetric, and small shoulders are present at the high-temperature sides of the peaks measured

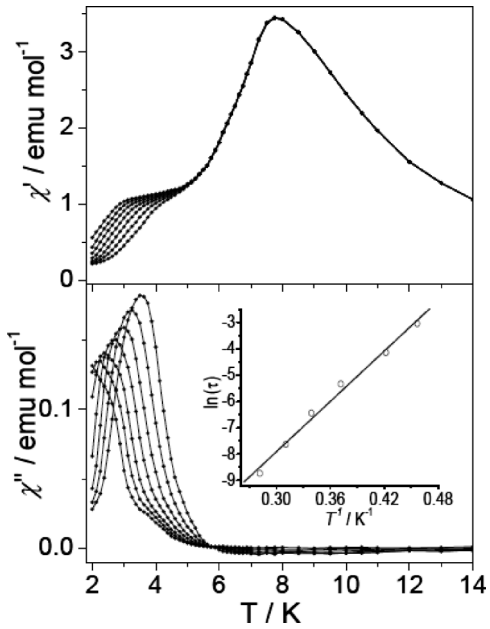

Fig. 7 Ac susceptibilities of **1** measured at frequencies of 1, 3, 10, 33, 100, 330 and 997 Hz under zero dc fields with a driving ac field of 3.5 Oe. Inset: temperature dependent relaxation time fitted to the Arrhenius equation.

at low frequencies. These may suggest the operation of multiple relaxation processes.[25] Therefore, the above-derived parameters for a single thermal activation process are rough approximations.

Considering the structural feature of **1**, it is most likely that the slow relaxation of magnetization in the AF phase arises from the SCM component (the FM and anisotropic Co(II) chains). The retention of SCM behaviors in AF phases has been experimentally and theoretically demonstrated recently in a few compounds.[9] The Glauber dynamics for Ising chains[26] predicts that $\Delta_\tau = 2\Delta_\xi$ for "infinite" chains and $\Delta_\tau = \Delta_\xi$ for "finite-size" chains.[1c,4b,27] For **1**, $\Delta_\tau < 2\Delta_\xi$, suggesting that the slow relaxation occurs in the "finite-size" regime, where the increase of ξ is limited by naturally occurring defects. The difference between Δ_τ and Δ_ξ can be justified by assuming that the spin flip in absence of magnetic exchange is also thermally activated with an anisotropy barrier, Δ_A. The activation barrier Δ_τ for relaxation depends not only upon the correlation energy Δ_ξ but also upon the single-ion anisotropy barrier Δ_A. For "finite-size" chains, $\Delta_\tau = \Delta_\xi + \Delta_A$. Thus, we get $\Delta_A = \Delta_\tau - \Delta_\xi = 9.7$ K. The comparison that $\Delta_A \ll \Delta_\xi$ indicates that broad domain walls are relevant in this system.[1c,20]

Isothermal ac measurements in the frequency range 0.1–1500 Hz were performed at 2.6 K. The χ''–χ' plot (Cole–Cole diagram) is highly dissymmetric, and seems to be an envelope of two semicircles corresponding to relaxation processes (Fig. 8). Thus we made attempts to fit the frequency-dependent data to the sum of two modified Debye functions:[28]

$$\chi(\omega) = \chi_S + (\chi_T - \chi_S)\left[\frac{\beta}{1+(i\omega\tau_1)^{1-\alpha_1}} + \frac{1-\beta}{1+(i\omega\tau_2)^{1-\alpha_2}}\right]$$

where β is the weight of the first process, and the other symbols have their usual meanings. The best-fit led to $\chi_T = 1.06$ emu mol^{-1}, $\chi_S = 0.19$ emu mol^{-1}, $\alpha_1 = 0.47$, $\tau_1 = 1.5 \times 10^{-3}$ s, $\alpha_2 = 0.50$, $\tau_1 = 0.16$ s and $\beta = 0.58$. The relatively large α values indicate a wide

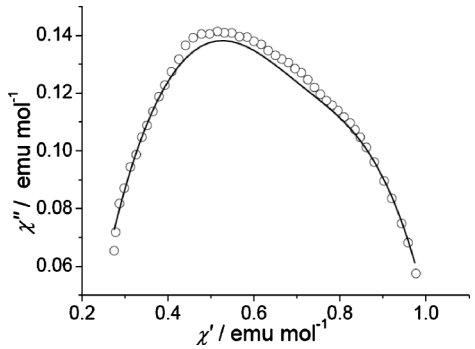

Fig. 8 Cole–Cole diagram of **1** at 2.6 K. The solid line is the best fit to the two-Debye-relaxation model.

distribution of relaxation time for both processes, but still lie in the range for reported SCMs.[4a] The occurrence of two separate relaxation processes may be related to the presence of two distinct types of anisotropic Co(II) sites along the chain (Co1 in the *cis*-octahedral $[N_2O_4]$ environment while Co2 and Co3 are in similar *trans*-octahedral $[N_2O_4]$ environments).[25a,c] Further investigations are needed to confirm the hypothesis, although it is well known that the relaxation rate is sensitive to the single-ion anisotropy and to variations of the coordination environment.[1c,29]

Compound **1** is similar to another Co(II) compound (**3**) reported recently by us,[9a] which is composed of 1D chains with the (μ-COO)$_2$(μ-N$_3$) triple bridge. They both exhibit intrachain FM coupling, interchain AF ordering, field-induced metamagnetic transition, and SCM-based slow dynamics. The Co–N–Co angles (av. 121.9(1)°) and Co···Co distances (av. 3.741(2) Å) for the Co(COO)(N$_3$)(O–H···O)Co bridging moieties in **1** are comparable to those (122.2(2)° and 3.659(1) Å) for Co(COO)$_2$(N$_3$)Co in **3**, but the intrachain FM coupling (J = 31.0 cm^{-1}) in **1** is significantly weaker than that (J = 54.1 cm^{-1}) in **3**. This suggests that the intrachain O–H···O hydrogen bond bridge is less efficient in promoting the FM interactions than the O–C–O carboxylate bridge. Importantly to the bulk magnetic behaviors, the interchain O–H···O bridge between Co(II) ions in **1** provides a short pathway (Co···Co distance, 5.98 Å) for interchain magnetic interactions, whereas the chains in **3** are much farther separated, the shortest Co···Co distance being 7.75 Å (associated with weak C–H···O hydrogen bonds). These structural differences may account for the higher AF ordering temperature and the higher metamagnetic critical field in **1** (T_c = 7.7 K and H_c = 950 Oe. For comparison, the data for **3** are 6.4 K and 100 Oe). Furthermore, the presence of two distinct types of Co(II) sites may be responsible for the complex relaxation processes in **1**. For comparison, there is only one independent Co(II) site in **3**, which shows a single relaxation process.

Compound 2. The χT value of **2** at 300 K (1.56 emu K mol^{-1}) is typical of Ni(II) systems with $g > 2$. Upon cooling, the χ and χT values increase smoothly to maxima at 5.9 and 7 K, respectively, and then drop rapidly (Fig. 9). The $1/\chi$ *vs.* T plot above 140 K obeys the Curie–Weiss law, with C = 1.31 emu mol^{-1} K and θ = 46.6 K. The positive θ value and the increase of χT with decreased temperature clearly indicate FM coupling between the Ni(II) ions.

According to structural data, the thermal magnetic data of **2** was analyzed using the polynomial expression for Ni(II) chains with alternating FM interactions: [30]

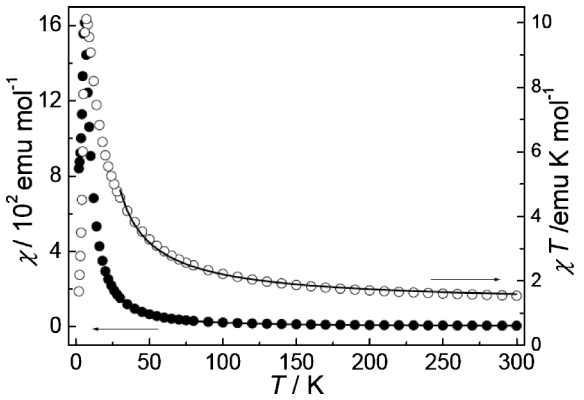

Fig. 9 Temperature dependence of χT and χ for **2** under 1 kOe. The solid lines represent the best fit to the appropriate model (see text).

$$H = -\sum(J_1 S_{2i} S_{2i+1} + J_2 S_{2i} S_{2i-1})$$

$$\chi = (2N\beta^2 g^2/3kT)\frac{AX^3 + BX^2 + CX + 1}{DX^2 + EX + 1}$$

where $X = J_1/kT$, and the coefficients A–E are polynomial functions of $\alpha = J_2/J_1$, The best fit of the data above 30 K produced J_1 = 34.4 cm^{-1}, J_2 = 29.9 K (α = 0.87) with g = 2.28. The FM interactions, confirmed by the positive J values, are consistent with previous studies on Ni(II) compounds with similar (COO)(N$_3$) bridges (J = 24–36 cm^{-1}).[7d,31]

The presence of the χ maximum at 5.9 K suggests the occurrence of long-range AF ordering of the FM chains. Further magnetization measurements performed under different fields (Fig. 10a) revealed that the maximum shifts to lower temperature as the field is increased and disappears at the high field of 3.0 kOe. The behaviors are characteristic of field-induced metamagnetism, and the disappearance of the maximum indicates that the interchain AF ordering is broken up by the field. The metamagnetic transition is confirmed by the sigmoidal shape of the isothermal magnetization curve measured at 2 K (Fig. 10b), from which the critical field (H_c) is estimated to be about 2.3 kOe. No evident hysteresis was observed upon cycling the field between −5 and 5 T at 2 K (Fig. S3, ESI†). Finally, the ac magnetic measurements were performed under zero dc field at different frequencies (Fig. S4, ESI†). The ac susceptibility exhibits a maximum in the real component (χ') at 6.2 K. No frequency dependency and no evident imaginary signal (χ'') were observed, typical of AF ordering.

Conclusions

We have described the structures and magnetic properties of two isomorphous compounds of formula [M(4,4-opybz)(N$_3$)(H$_2$O)]$_n$ (4,4-opybz = 4-(4-pyridyl)benzoate *N*-oxide, M = Co, **1** and Ni, **2**). In the compounds, metal ions are linked into chains by simultaneous μ-EO-N$_3$, *syn*,*syn*-COO and O–H···O bridges, and the chains are interlinked by the backbones of the 4,4-opybz ligands into 2D coordination layers. The structure also features interchain O–H···O bridges between metal ions. Both compounds exhibit FM interactions through the intrachain (μ-N$_3$)(μ-COO)(O–H···O) bridges and AF interactions through the interchain O–H···O bridges. The FM chains are AF ordered, and

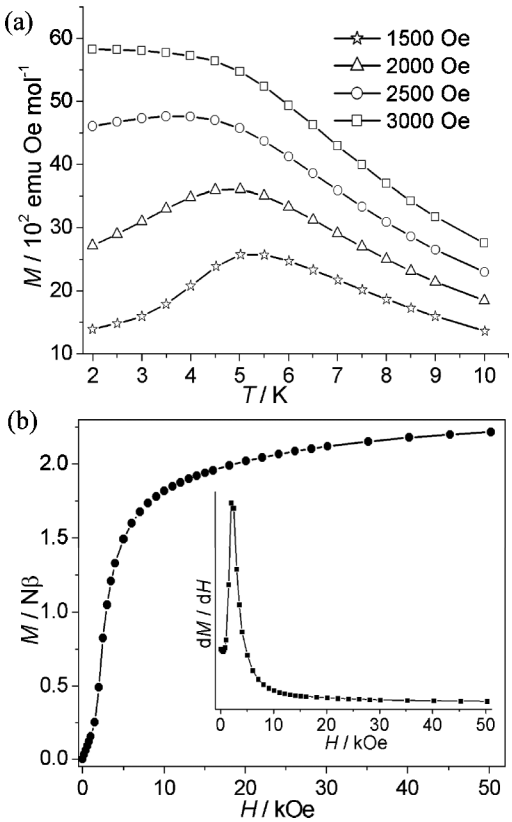

Fig. 10 (a) FC magnetization curves for **2** at different fields. (b) Isothermal magnetization curves at 2 K for **2**.

the AF phases exhibit a field-induced metamagnetic transition. However, **1** displays SCM-based slow relaxation of magnetization, while **2** does not. The SCM dynamics in AF ordered phases is still a rare occurrence. The difference between the Ni(II) and Co(II) compounds emphasizes the great importance of large magnetic anisotropy for SCM dynamics. As is well known, the octahedral Ni(II) system has a small magnetic anisotropy, which originates from zero-field splitting associated with second-order spin–orbital coupling, while Co(II) has a large magnetic anisotropy due to the first-order spin-orbit coupling related to the unquenched orbital momentum. Furthermore, more than one relaxation process is operative in the Co(II) compound, which is likely to be associated with the presence of distinct anisotropic sites.

Acknowledgements

This work is supported by NSFC (91022017) and the Fundamental Research Funds for the Central Universities.

References

1 (*a*) O. Kahn, *Molecular Magnetism*, VCH, New York. 1993; (*b*) J. Ribas, A. Escuer, M. Monfort, R. Vicente, R. Cortes, L. Lezama and T. Rojo, *Coord. Chem. Rev.*, 1999, **193–195**, 1027; (*c*) C. Coulon, H. Miyasaka and R. Clérac, *Struct. Bonding*, 2006, **122**, 163; (*d*) D. Gatteschi, O. Kahn, J. S. Miller and F. Palacio, *Magnetic Molecular Materials*, Kluwer Academic, Dordrecht, The Netherlands,1991.

2 (*a*) J. S. Miller, *Adv. Mater.*, 2002, **14**, 1105; (*b*) D. Gatteschi and R. Sessoli, *Angew. Chem., Int. Ed.*, 2003, **42**, 268; (*c*) J. S. Miller and A.-J. Epstein, *Angew. Chem., Int. Ed. Engl.*, 1994, **33**, 385; (*d*) *Magnetism: Molecules to Materials*; ed. J. S. Miller and M. Drilon, Willey-VCH, Weinheim, 2002–2005, vol. I–V; (*e*) J. S. Miller and A. J. Epstein, *Angew. Chem.*, 1994, **106**, 399.

3 (*a*) R. L. Carlin, *Magnetochemistry*, Springer, Berlin-Heidelberg, 1986; (*b*) B. Deviren and M. Keskin, *Phys. Lett. A*, 2010, **374**, 3119; (*c*) N. Motokawa, S. Matsunaga, S. Takaishi, H. Miyasaka, M. Yamashita and K. R. Dunbar, *J. Am. Chem. Soc.*, 2010, **132**, 11943.

4 (*a*) H.-L. Sun, Z.-M. Wang and S. Gao, *Coord. Chem. Rev.*, 2010, **254**, 1081; (*b*) L. Bogani, A. Vindigni, R. Sessoli and D. Gatteschi, *J. Mater. Chem.*, 2008, **18**, 4750; (*c*) T. Liu, Y.-J. Zhang, S. Kanegawa and O. Sato, *J. Am. Chem. Soc.*, 2010, **132**, 8250; (*d*) T. D. Harris, M. V. Bennett, R. Cléracand and J. R. Long, *J. Am. Chem. Soc.*, 2010, **132**, 3980; (*e*) C. I. Yang, Y. J. Tsai, S. P. Hung, H. L. Tsai and M. Nakano, *Chem. Commun.*, 2010, **46**, 5716.

5 (*a*) E. Pardo, C. Train, R. Lescouëzec, Y. Journaux, J. Pasán, C. Ruiz-Pérez, F. S. Delgado, R. Ruiz-Garcia, F. Lloret and C. Paulsen, *Chem. Commun.*, 2010, **46**, 2322; (*b*) T. C. Stamatatos, K. A. Abboud, W. Wernsdorfer and G. Christou, *Inorg. Chem.*, 2009, **48**, 807; (*c*) D. Visinescu, A. M. Madalan, M. Andruh, C. Duhayon, J. P. Sutter, L. Ungur, W. V. Heuvel and L. F. Chibotaru, *Chem.–Eur. J.*, 2009, **15**, 11808.

6 (*a*) A. Saitoh, H. Miyasaka, M. Yamashita and R. Clérac, *J. Mater. Chem.*, 2007, **17**, 2002; (*b*) A. Caneschi, D. Gatteschi, N. Lalioti, C. Sangregorio, R. Sessoli, G. Venturi, A. Vindigni, A. Rettori, M. G. Pini and M. A. Novak, *Angew. Chem., Int. Ed.*, 2001, **40**, 1760; (*c*) R. Clérac, H. Miyasaka, M. Yamashita and C. Coulon, *J. Am. Chem. Soc.*, 2002, **124**, 12837 .

7 (*a*) Q.-X. Jia, H. Tian, J.-Y. Zhang and E.-Q. Gao, *Chem.–Eur. J.*, 2011, **17**, 1040; (*b*) T. Liu, Y.-J. Zhang, Z.-M. Wang and S. Gao, *Inorg. Chem.*, 2006, **45**, 2782; (*c*) W.-W. Sun, C.-Y. Tian, X.-H. Jing, Y.-Q. Wang and E.-Q. Gao, *Chem. Commun.*, 2009, 4741; (*d*) Z. He, Z.-M. Wang, S. Gao and C.-H. Yan, *Inorg. Chem.*, 2006, **45**, 6694.

8 (*a*) H. Miyasaka, K. Takayama, A. Saitoh, S. Furukawa, M. Yamashita and R. Clérac, *Chem.–Eur. J.*, 2010, **16**, 3656; (*b*) C. Coulon, R. Clérac, W. Wernsdorfer, T. Colin and H. Miyasaka, *Phys. Rev. Lett.*, 2009, **102**, 167204.

9 (*a*) X.-M. Zhang, Y.-Q. Wang, K. Wang, E.-Q. Gao and C.-M. Liu, *Chem. Commun.*, 2011, **47**, 1815; (*b*) Y.-Q. Wang, W.-W. Sun, Z.-D. Wang, Q.-X. Jia, E.-Q. Gao and Y. Song, *Chem. Commun.*, 2011, **47**, 6386.

10 (*a*) Y. Ma, J.-Y. Zhang, A.-L. Cheng, Q. Sun, E.-Q. Gao and C.-M. Liu, *Inorg. Chem.*, 2009, **48**, 6142; (*b*) Y.-Q. Wang, Q.-X. Jia, K. Wang, A.-L. Cheng and E.-Q. Gao, *Inorg. Chem.*, 2010, **49**, 1551; (*c*) Y. Ma, Y.-Q. Wen, J.-Y. Zhang, E.-Q. Gao and C.-M. Liu, *Dalton Trans.*, 2010, **39**, 1846; (*d*) C.-Y. Tian, W.-W. Sun, Q.-X. Jia, H. Tian and E.-Q. Gao, *Dalton Trans.*, 2009, 6109.

11 (*a*) Y. Ma, N. A. G. Bandeira, V. Robert and E.-Q. Gao, *Chem.–Eur. J.*, 2011, **17**, 1988; (*b*) Y. Ma, K. Wang, E.-Q. Gao and Y. Song, *Dalton Trans.*, 2010, **39**, 7714; (*c*) Y.-Q. Wang, J.-Y. Zhang, Q.-X. Jia, E.-Q. Gao and C.-M. Liu, *Inorg. Chem.*, 2009, **48**, 789; (*d*) Y. Ma, X.-B. Li, X.-C. Yi, Q.-X. Jia, E.-Q. Gao and C.-M. Liu, *Inorg. Chem.*, 2010, **49**, 8092.

12 (*a*) J.-P. Zhao, B.-W. Hu, Q. Yang, X.-F. Zhang, T.-L. Hu and X.-H. Bu, *Dalton Trans.*, 2010, **39**, 56.

13 (*a*) X.-T. Wang, X.-H. Wang, Z.-M. Wang and S. Gao, *Inorg. Chem.*, 2009, **48**, 1301; (*b*) A. K. Boudalis, M. Pissas, C. P. Raptopoulou, V. Psycharis, B. Abarca and R. Ballesteros, *Inorg. Chem.*, 2008, **47**, 10674.

14 I. Wolfle, J. Lodaya, B. Sauerwein and G. B. Schuster, *J. Am. Chem. Soc.*, 1992, **114**, 9304.

15 *Theory and Application of Molecular Diamagnetism*, ed. E. A. Boudreaux and J. N. Mulay, J. Wiley and Sons, New York, 1976.

16 G. M. Sheldrick, *Program for Empirical Absorption Correction of Area Detector Data*, University of Göttingen, Göttingen, Germany, 1996.

17 G. M. Sheldrick, *SHELXTL*, version 5.1., Bruker Analytical X-ray Instruments Inc., Madison, WI, 1998.

18 J. Laugier and B. Bochu, *LMGP-Suite Suite of Programs for the interpretation of X-ray Experiments*, ENSP/Laboratoire des Matériaux et du Génie Physique, Saint Martin d'Hères, France. http://www.inpg.fr/LMGP and http://www.ccp14.ac.uk/tutorial/lmgp/.

19 M. C. Etter, *Acc. Chem. Res.*, 1990, **23**, 120.

20 C. Coulon, R. Clérac, L. Lecren, W. Wernsdorfer and H. Miyasaka, *Phys. Rev. B: Condens. Matter Mater. Phys.*, 2004, **69**, 132408.

21 E. Ising, *Zeitschrift für Physik*, 1925, **31**, 253.

22 J. H. Luscombe, *Phys. Rev. B*, 1987, **36**, 501.
23 (*a*) D. Chowdhury, *Spin Glasses and Other Frustrated Systems*, Princeton University Press, New Jersey, 1986; (*b*) J. A. Mydosh, *Spin Glasses: An Experimental Introduction*, Taylor & Francis, London, 1993.
24 J. H. Yoon, D. W. Ryu, H. C. Kim, S. W. Yoon, B. J. Suh and C. S. Hong, *Chem.–Eur. J.*, 2009, **15**, 3661.
25 (*a*) Y.-N. Guo, G.-F. Xu, P. Gamez, L. Zhao, S.-Y. Lin, R. Deng, J.-K. Tang and H.-J. Zhang, *J. Am. Chem. Soc.*, 2010, **132**, 8538; (*b*) I. Hewitt, Y. H. Lan, C. E. Anson, J. Luzon, R. Sessoli and A. K. Powell, *Chem. Commun.*, 2009, 6765; (*c*) P.-H. Lin, T. J. Burchell, L. Ungur, L. F. Chibotaru, W. Wernsdorfer and M. Murugesu, *Angew. Chem., Int. Ed.*, 2009, **48**, 9489.
26 R. J. Glauber, *J. Math. Phys.*, 1963, **4**, 294.
27 L. Bogani, A. Caneschi, M. Fedi, D. Gatteschi, M. Massi, M. A. Novak, M. G. Pini, A. Rettori, R. Sessoli and A. Vindigni, *Phys. Rev. Lett.*, 2004, **92**, 207204.
28 S.-D. Jiang, B.-W. Wang, H.-L. Sun, Z.-M. Wang and S. Gao, *J. Am. Chem. Soc.*, 2011, **133**, 4730.
29 M. Gonidec, F. Luis, À. Vílchez, J. Esquena, D. B. Amabilino and J. Veciana, *Angew. Chem., Int. Ed.*, 2010, **49**, 1623.
30 M. Monfort, I. Resino, M. S. E. Fallah, J. Ribas, X. Solans, M. Font-Bardia and H. Stoeckli-Evans, *Chem.–Eur. J.*, 2001, **7**, 280.
31 (*a*) B.-W. Hu, J.-P. Zhao, E. C. Sañudo, F.-C. Liu, Y.-F Zeng and X.-H. Bu, *Dalton Trans.*, 2008, 5556; (*b*) F.-C. Liu, Y.-F. Zeng, J.-R. Li, X.-H. Bu, H.-J. Zhang and J. Ribas, *Inorg. Chem.*, 2005, **44**, 7298.